SSC16-WK-44

CubeSat Nighttime Lights

Dee W. Pack, Brian S. Hardy
The Aerospace Corporation
2310 E. El Segundo Blvd, El Segundo, CA 90245; 310-336-5645
dee.w.pack@aero.org

ABSTRACT

Monitoring of visible emissions at night from satellites has evolved into a useful capability for environmental monitoring and mapping the global human footprint. Pioneering work with Defense Meteorological Support Program (DMSP) sensors has been followed by new work with the Visible Infrared Imaging Radiometer Suite (VIIRS), and International Space Station (ISS) photography. We have been investigating the ability of CubeSats to carry out nightlights mapping missions and here present recent results from existing visible wavelength cameras on AeroCube satellites. CubeSat sensors were successfully tasked to image oil industry natural gas flares in the Persian Gulf region, urban areas and other sites of interest. Point and stare maneuvers to maximize resolution and sensitivity were demonstrated. Our initial work demonstrates the ability of CubeSats to conduct nightlights missions, as well as the limitations of the small cameras flown to date. Comparison of VIIRS and AeroCube imagery are made. Potential uses of the CubeSat platforms include: 1) providing different overpass times than the early morning overpass provided by VIIRS to potentially spot missing lights activity, 2) providing multi-color nightlights to supplement the monochromatic VIIRS day-night-band (DNB) data, and 3) "swarming" the nighttime mission with multiple platforms to provide more frequent tasked data on transient events such as fires, volcanic activity, and natural disaster power outages. CubeSats sensors may be able to improve mapping of the human footprint in targeted regions via nighttime lights and contribute to better monitoring of: urban growth, light pollution, energy usage, the improvement of electrical power grids in developing countries, and oil industry flare activity. Future CubeSats sensors should be able to contribute to nightlights monitoring efforts by NOAA, NASA, ESA, the World Bank and others. Our current results are summarized and next steps discussed, including soon-to-be-launched sensors and future program development.

1.0 Introduction

The use of CubeSats for Earth remote sensing applications requires missions for which spatial resolution is not the highest priority, and for which the targets are fairly bright. Imaging the Earth at night can provide such remote sensing targets – bright city lights, bright natural gas flares and fires. Monitoring human lighting is a sensitive way of mapping the human footprint and charting urban growth and energy usage. Gas flares are of interest as metric pointing targets and can be exceptionally bright. Flares around the world are also important contributors to global CO2 emissions and are indicators of oil industry expansion, contraction and conservation efforts, making them attractive science targets. Lights and industrial flares are also important economic indicators and studying their activity levels, on/off status and interruption by natural disasters, and other changes is of significance for country and industry studies.

The nightlights mission was pioneered by the Defense Meteorological Support Program (DMSP) Operational Line Scanner (OLS) at 2.5 km resolution and enhanced since 2012 by the Visible Infrared Imaging Radiometer Suite (VIIRS) Day/Night band (DNB) at .74 km resolution. Dr. Chris Elvidge and colleagues have created well-georegistered global databases of nighttime lights and flares from comprehensive work with DMSP and VIIRS.[1-6] We were guided by these NOAA databases and chose to monitor some of these well-studied sites with CubeSat sensors for comparison to the VIIRS DNB. Our CubeSats flew simple CMOS cameras with small lenses, but allowed higher resolution images than the VIIRS DNB payload. Regions studied included Kuwait City and the Persian Gulf area, which feature oil industry natural gas flares, as well as widespread city lights and cooperative, often cloud-free weather.

Through studying nightlights data from existing uncalibrated AeroCube cameras, and higher quality, soon-to-be flown calibrated AeroCube cameras, we intend to demonstrate the ability of CubeSats in this mission area and gain experience to aid in designing a future more capable sensor which could be termed a NightCube. Should continuing the nighttime lights monitoring capability prove difficult for future weather satellite programs, CubeSats offer the possibility of a

low-cost option to continue aspects of this mission. In addition, a NightCube mission could offer an affordable means to supplement or compliment future nightlights sensors through different orbits and temporal coverage, and different spectral and spatial sensor characteristics. SmallSats have also been proposed for this mission area, notably the NOAA/NASA Nightsat effort to which we will refer when discussing requirements and performance parameters.

2.0 AEROCUBE SENSORS

The satellites used in this initial work were AeroCube-4 and AeroCube-5. AC-4 and AC-5 are both 3-axis stabilized CubeSats built by The Aerospace Corporation in the 1U and 1.5U form factor, respectively. AC-4 flew three cameras: wide (fish eye), medium and narrow field of view (FOV). AC-5 flew only a narrow FOV camera (identical to AC-4's). Only results from AC-4 MFOV and AC-5 NFOV cameras are reported in this paper. Table 1 summarizes some important parameters of these small cameras.

Table 1. Camera Parameters

Satellite Camera	Lens F#	Lens FL (mm)	Pixel Pitch (µm)	Nominal Altitude (km)	GSD (m)
AC-4 (MFOV)	2	3.40	2.80	600	494
AC-5 (NFOV)	2	15.8	2.80	700	124

The camera sensor chips in both AC-4 and AC-5 were Aptina MT9D131 1600x1200 pixel 10-bit color RGB Bayer pattern CMOS arrays. These chips are very compact, reasonably low noise devices designed for use in machine vision and security camera applications and have decent low light sensitivity. Based on the manufacturer's specifications, the quantum efficiencies for the RGB channels peak at 37%, and the full width at half maximum (FWHM) band pass for all three channels is approximately 400-850 nm. The individual channels are: R=560-850 nm, G=480-590 nm, B=400-512 nm FWHM. These cameras were included on the AC-4 and AC-5 missions to provide an unambiguous reference for calibration of the attitude-control system and were neither designed nor calibrated with a dedicated science mission in mind. Autoexposure was the only camera mode available for operations and images were downlinked using jpeg compression. Additional information on these CubeSats has been summarized in several papers by Gangestad and co-workers, including their use for daytime remote sensing observations of forest fires, sun glint and a solar eclipse.[7-9] Despite their limitations, the tiny cameras proved capable of taking nighttime images of city lights and oil industry gas flares, particularly when tasked to point and stare at a target location, which improved the resolution and sensitivity.

2.1 Imaging the Persian Gulf with AeroCube-4

In 2014, we began tasking cameras flying on AeroCube-4 to collect experimental nighttime imagery over the Persian Gulf and surrounding areas. Initial "fly-and-shoot" pictures were encouraging enough that we programmed a careful experiment to target nighttime imagery of Kuwait City and the surrounding oil and gas field flares. This entailed programming the AC-4 spacecraft to obtain Earth and Sun lock on the sunlit side of the Earth, orbiting across the terminator and then taking pictures in a sequence on the way towards our target, the bright lights of Kuwait City and the nearby extremely bright gas flares. Once over the specified coordinates, the spacecraft would then continue to take images while actively pointing at Kuwait City. After several tries, we succeeded in this attempt, with example results shown in Figures 1 and 2.

Figure 1 shows a pointing stabilized, full 1600x1200 pixel, contrast-stretched AC-4 image of the Northern Persian Gulf centered over Kuwait City compared to VIIRS data from the same night taken only 20 minutes later. The autoexposure time was approximately 0.3 seconds, as we show via streak analysis of the pre- and post-pointing maneuver frames in Figure 2 and in the accompanying discussion. The notable bright features on the North side of the image are the so-called "string of pearls", which are very bright gas flares from gas oil separation plants near Basra in Iraq. These bright features, and other gas flares in the Gulf region are almost always emitting, and provide good pointing fiducial sources for space sensor metric calibration. Most of the bright features detected in the VIIRS DNB were also detected in the AC-4 MFOV camera image. Our initial impression was that this result was rather extraordinary, and we were pleased that an image from a small aperture staring camera on a 1.3kg, 1U CubeSat could be reasonably compared to a portion of the 3000 km wide swath of the much more sophisticated spinning day-night-band sensor on the Suomi NPP spacecraft (2200 kg, 1400 kg dry). A more careful comparison shows the remarkable sensitivity and excellent calibration of the VIIRS DNB sensor far outperforming the AC-4 CMOS sensor at low intensities. This is evident when comparing the moonlit desert and the land/sea boundary that is barely visible in the AC-4 image in Fig.1. The signal contrast between the moonlit desert and dark ocean surfaces provides a useful approximation of the sensitivity of the AC-4 camera. The jpeg image values are consistent with a desert-to-dark Persian Gulf contrast ratio of approximately 2:1 across the R and G channels with the water signal mostly noise (the blue channel in the RGB

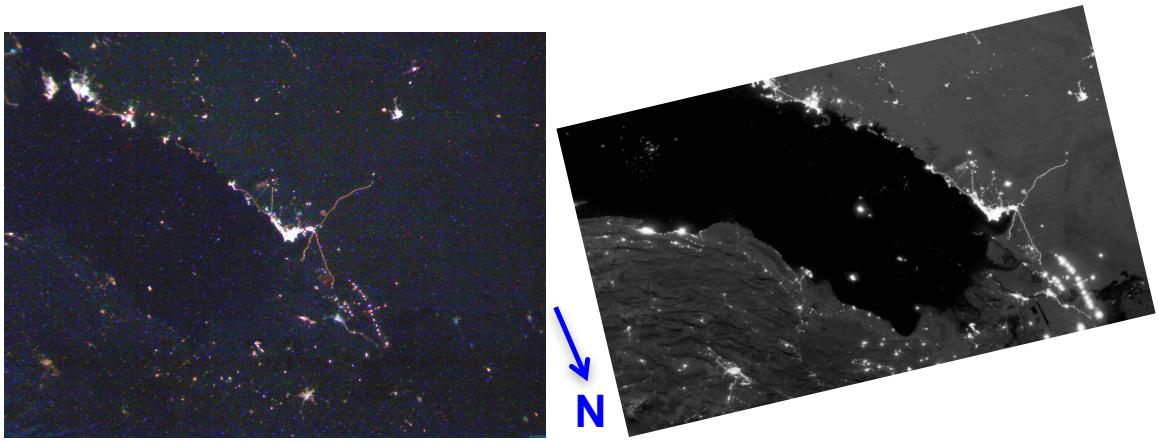

A B

Figure 1. Comparison of Persian Gulf Nighttime Lights Data. A. Left - AC-4 MFOV camera 11 July 2014 22:30:03 UT. B. Right - VIIRS day-night-band sensor 11 July 2014 22:50:04 UT. Lunar data were: 22:30 UT Altitude 32.2°, Azimuth 218°; 22:50 UT Altitude 29.5°, Azimuth 222° with the Moon Phase at 99% illumination. (VIIRS Data are Courtesy of Chris Elvidge, NOAA and Kimberly Baugh, Cooperative Institute for Research in Environmental Sciences, University of Colorado).

image is noisier than the R and G and shows a lower SNR). The signal from the desert shows a signal-to-noise ratio of between 1 and 2 for the 3 channels. The calibrated VIIRS DNB shows a desert-to-dark Persian Gulf ratio of approximately 8-to-1.6 nW-cm^{-2}-sr^{-1}. The VIIRS bandpass is 505–890 nm FWHM. We conclude that the detection threshold for the AC-4 MFOV camera is certainly no better than the signal from the VIIRS-measured moonlit desert surface value of 8 nW-cm^{-2}-sr^{-1}, and is approximately 20 nW-cm^{-2}-sr^{-1} to achieve an SNR of around 4 or better. This is confirmed when comparing easily detected lights on isolated roads detected by AC-4 in the desert west of Kuwait City to the same roads in the VIIRS image which measures radiance values in the 20's of nW-cm^{-2}-sr^{-1}. Conversely dim lights seen in VIIRS below this threshold, such as the 12 nW-cm^{-2}-sr^{-1} lights on the bridge linking Saudi Arabia to Bahrain, were not definitively detected by AC-4, though the bright lights from a causeway island feature were evident. The brightest feature in the scene, and one of the brightest in world, is one of the Rumaila gas-oil separation plant flare complexes at 30.215N, 47.394E. This source has a VIIRS radiance of 54217 nW-cm^{-2}-sr^{-1}. The flare complex is ranked 10th in the world in the size of its estimated CO_2 emissions.[2] This same feature shows 8-bit jpeg RGB values of 255, 249, 255 in the AC-4 camera data indicating that the 8 bits are being filled efficiently. No other source in the scene saturates, or almost saturates, the AC-4 camera in this manner, though all of the "string-of-pearls features" are very bright. The original RGB Bayer pattern spatial sampling of the scene accounts for the fact that not all three channels were saturated.

To pursue these radiometric comparisons much further is difficult, given the lack of calibration of the AC-4 sensor RGB channels, the lack of raw data files, the truncation of the 10-bit data to 8-bit jpegs images, and would require a more thorough analysis of the VIIRS DNB nighttime data and its observational geometry and calibration. It is interesting, however, to compare these rough numbers to the spectral radiance sensitivity conclusions of the Nightsat mission concept paper authored by Elvidge and co-workers. They wrote: "The primary findings of our study are that Nightsat should collect data from a near-synchronous orbit in the early evening with 50 to 100 m spatial resolution and have spectral radiance detection limits of 25 nW-cm^{-2}-sr^{-1}-μm^{-1} or better".[10] We come fairly close, but do not achieve, the upper limit of these metrics with our CubeSat utility cameras without this having been the original purpose for these devices. In the years since the 2007 Nightsat paper was written, research with the VIIRS DNB has given us an enhanced appreciation of nightlights sensitivities, as it outperformed the original mission design by an impressive margin.[3,4] None-the-less, the ability to see down to full moon illumination can be considered the upper limit of sensitivity at which nightlight images of urban scenes in the visible wavelength range begin to become useful. We explore this further in section 2.3 and show results from the higher resolution NFOV camera on the more readily pointed AC-5 spacecraft. First, we discuss in more detail the point-and-stare experiment of 11 July 2014 and compare smeared and pointing stabilized nighttime lights imagery.

2.2 Details of the Point-and-Stare Experiment with AeroCube-4

The AC-4 Persian Gulf collection pass for this experiment started over Baghdad and took a sequence of images in push broom mode every 5 seconds until the sensor orbited South directly over Kuwait City. At that position, AC-4 was programmed to stay pointed at Kuwait City to reduce smear and obtain optimal images. The sensor continued to image every 5 seconds until the Earth horizon rose. Figure 2 shows a detailed portion of the near-nadir pre- and post-pointing maneuver images of the "string of pearls" gas flare features. Note that some uncorrected pattern noise is evident in these stretched images. The streaks from the bright gas flares in the pre-pointing maneuver frame are clearly evident. The length of these streaks average to about 5 pixels. The pixel size is calculated from known distances between the bright gas flares as ~470 m. This compares very closely with the result calculated from the optical parameters of the MFOV camera, the modest off-nadir angle and the orbital altitude of the AC-4 spacecraft (561 km) during this experiment.

Using the appropriate orbital velocity of 7.7 km/sec we calculate an exposure of about 0.3 seconds for the images taken in this experiment based on the streaks. The improvement in image quality and sensitivity from this spacecraft-pointing stabilization maneuver is clearly illustrated. Testing the performance of this pointing maneuver was one goal of our nighttime experiments. This point and stare procedure became our normal tasking method for nighttime data collection with the AeroCube cameras when image quality was desired, including all of the AC-5 data which follow. The utility of gas flares as beacons for testing precision spacecraft pointing maneuvers, a goal of recent and future AeroCube missions, is also evident in Figure 2.

The estimate the autoexposure time of the AC-4 camera in this experiment is useful for understanding the performance of future, more sensitive cameras. We used this exposure time in calculating expected signals from MODTRAN and Lunar model predictions of the illuminated desert and ocean surfaces.

2.3 AeroCube-5 Experiments

We followed these observations with additional nighttime tasking using the easier-to-point AC-5 1.5U CubeSat. It is useful to review some aspects of the pointing capabilities of the AeroCube satellites. The AeroCube-4 satellite's attitude control system (ACS) does not use a rate gryo, relying completely on its Earth, Sun, and magnetic field sensors. At best, these sensors can provide pointing capability to within a degree of accuracy, however the typical accuracy is a few degrees. In the example shown above the pointing accuracy achieved was approximately 3 degrees, with the achieved image center about 29 km off the coast of Kuwait City, the intended target. Further, these sensors do not always provide a sufficient solution for the attitude control system, so AC-4 cannot achieve arbitrary attitudes. For nighttime images, when the sun must be below the horizon, pointing is especially difficult because of the lack of inputs to the sun sensor. As a result, the satellite typically loses attitude knowledge a few minutes into eclipse. This constraint means that AC-4 was only able to attempt nighttime images over a particular target a few days every few months because the orbit must pass over the target soon after the satellite passes into eclipse, and the success rate during these opportunities is low.

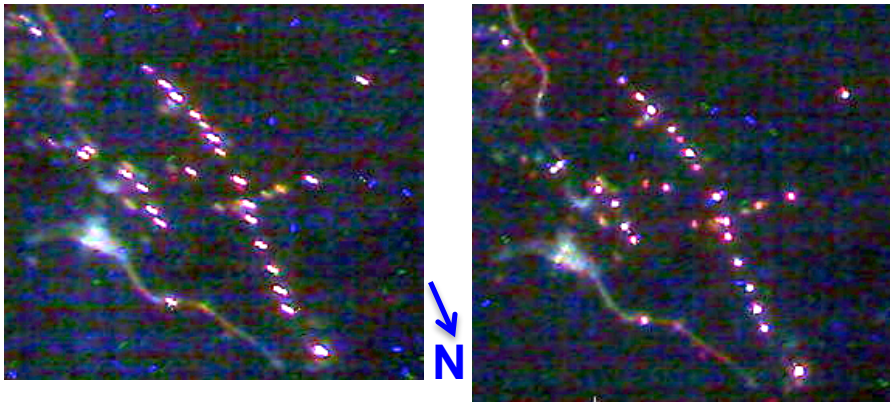

Figure 2. Detail of the Basra "string-of-pearls" gas flare region in Iraq from the pre- and post-pointing maneuver frames. A. Frame 8 – just prior to the pointing maneuver. B. Frame 9 - just after the pointing maneuver. Basra is on the lower left side of the image chip. Road features are evident in addition to the gas flares. This is a detail of the full scene in Fig. 1A, frame 9 in the pointing sequence experiment.

Because of the limited opportunities and the low success rate of nighttime tasking by AC-4, AC-5-A was used instead, when it was not performing other experiments. AeroCube-5-A possesses the same ACS sensor suite as AC-4 with the addition of a rate gyro. The rate gyro allows the satellite to maintain attitude control throughout eclipse, relying on the stability of the gyro's measurements for its attitude knowledge. The satellite initializes its attitude control system using its earth and sun sensors, and estimates the stability and drift of the gyro's measurements prior to entering into eclipse. The error in pointing grows throughout the period of time in eclipse, and varies from case to case. As a result, images taken later in eclipse generally have poorer aim than those taken earlier in eclipse, and sometimes miss the target completely.

Future AeroCube satellites that require continuous sub-degree pointing accuracy will use the newly developed star camera system, which will fly on the AeroCube-7 satellites and ISARA. The star camera system is able to provide updates to the attitude control system every few seconds, so instead of relying on the gyro stability for tens of minutes, it will only need to rely on the gyro stability for seconds. This capability is expected to improve pointing performance from a few degrees down to a few hundredths of a degree, independent of whether the satellite is in sunlight or eclipse.

The experiments we carried out with AC-5 were different from the AC-4 experiment described above. Instead of taking a series of images on the way to an aim point, and then pointing and staring, we tasked the satellite to stare at several targets along its orbital path in sequence, or merely to stare at one target and take several images. A target list of cities and oil industry sites was prepared, guided by recent VIIRS, DMSP and ISS camera research. Some highlights follow.

2.4 Persian Gulf AeroCube-5 Experiments

Figure 3 shows a sequence of NFOV camera frames from an AC-5 flyover of the Persian Gulf on 11 May 2015 in comparison to the previously presented 11 July 2014 AC-4 MFOV camera image superimposed using Google Earth. This gives a good comparison of the FOV of the two cameras whose parameters were summarized in Table 1. Both cameras share the same 1600x1200 pixel CMOS sensor, but have different focal length *f*/2 lenses, and have approximately 790x590 km and 200x150 km footprints. The programmed sequence for this AC-5 experiment was: point at Qatar for several frames, wait, point at Kuwait City for several frames, wait, then point at the Basra gas flares for two frames. The timing was slightly off, but the objectives of the experiment to demonstrate targeted tasking for nightlights mapping was achieved.

Figure 4 shows two images taken during the 11 May 2015 experiment with the AC-5 NFOV camera: A. Qatar/Bahrain and B. Kuwait City/Iraqi border region. The first image shows the nightlights of most of the Qatar peninsula, Bahrain and a small portion of the Saudi Arabian coastline near the city of Khobar. The second image in Figure 4 shows a higher resolution look at the same Kuwait/Iraq border region studied with the AC-4 MFOV camera. More nightlights details are evident in these images due to the higher resolution of the NFOV camera. Desert roads, neighborhood boundaries, gas flares and other features, such as bright oval racetracks in Qatar, are evident. White and green-blue regions lit by mercury vapor, fluorescent, metal-halide or LED lamps are distinct from the yellow-orange color of sodium vapor lighting. The images show features similar to those seen in ISS nighttime photography pioneered by NASA's Dan Pettit and more recently by the European Space Agency NightPod instrument onboard the ISS.[10,11] The ISS efforts used high-end Nikon cameras and programmable mechanisms to compensate for the space station's orbital motions. We accomplish a similar result with the reaction wheels and INS of the tiny AeroCube spacecraft. The moon was past last quarter in the 11 May 2015 experiment and low on the horizon such that its brightness was down by approximately a factor of 50 or more from the full moon. Unsurprisingly, no evidence of surface scattered moonlight appears in these images, unlike those in Figure 1. Examination of nightlight features shows that the AC-5 NFOV camera detected the same 20 nW-cm^{-2}-sr^{-1} road features as the WFOV AC-4 camera, and did not definitively detect the Saudi-Bahrain bridge lights at the ~10n nW-cm^{-2}-sr^{-1} level predicted from VIIRS data, though the brighter causeway island features are detected and clearly resolved. Since the pixel pitch and f-number are the same for the MFOV and NFOV cameras, their light gathering power is the same and their sensitivity is expected to be similar or identical. This proved to be the case in practice, though the AC-5 camera appeared to be less noisy with less fixed pattern noise, perhaps due to the aging of the AC-4 camera in space.

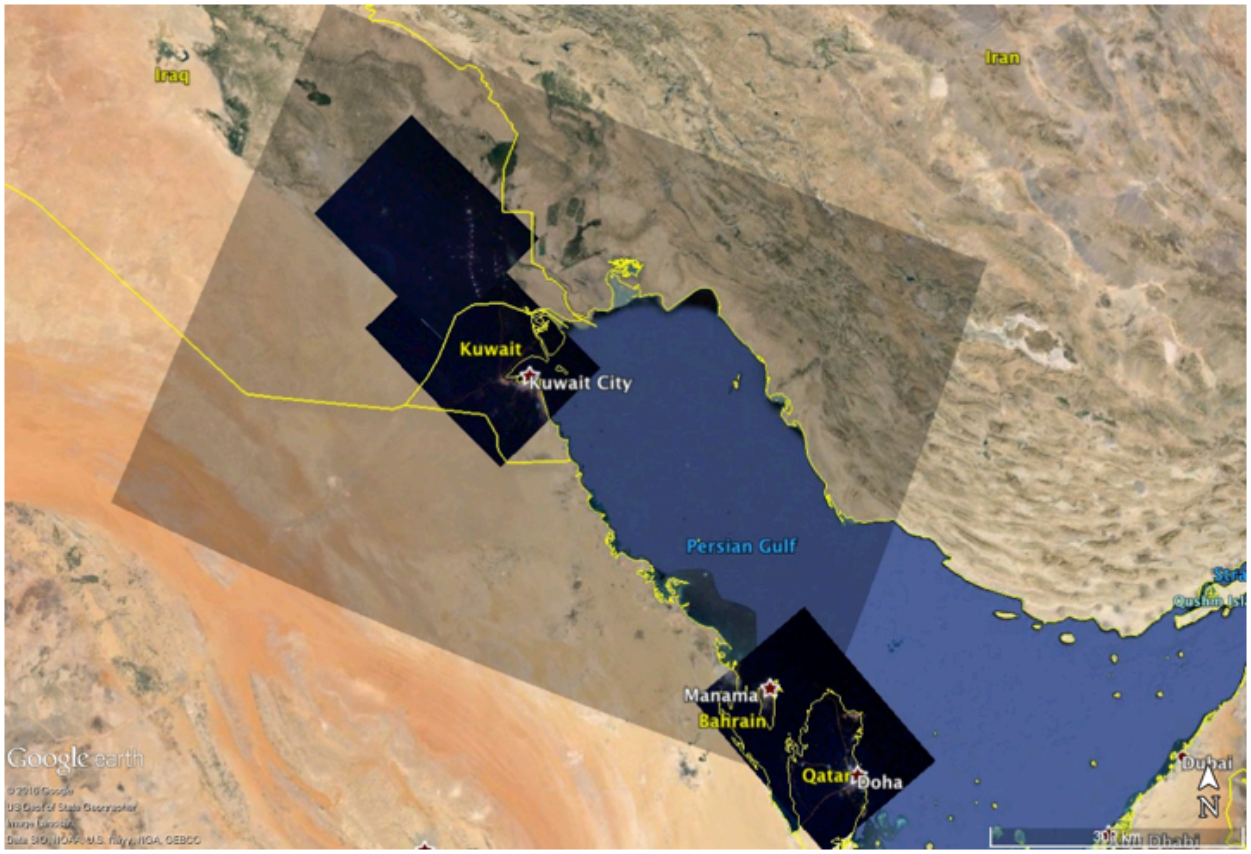

Figure 3. The Persian Gulf Region with Overlaid AeroCube Camera Fields of View. 3 Frames from the 11 May 2015 AC-5 NFOV Camera Flyby Experiment are Depicted with the Larger 11 July 2014 AC-4 MFOV Camera Footprint Superimposed.

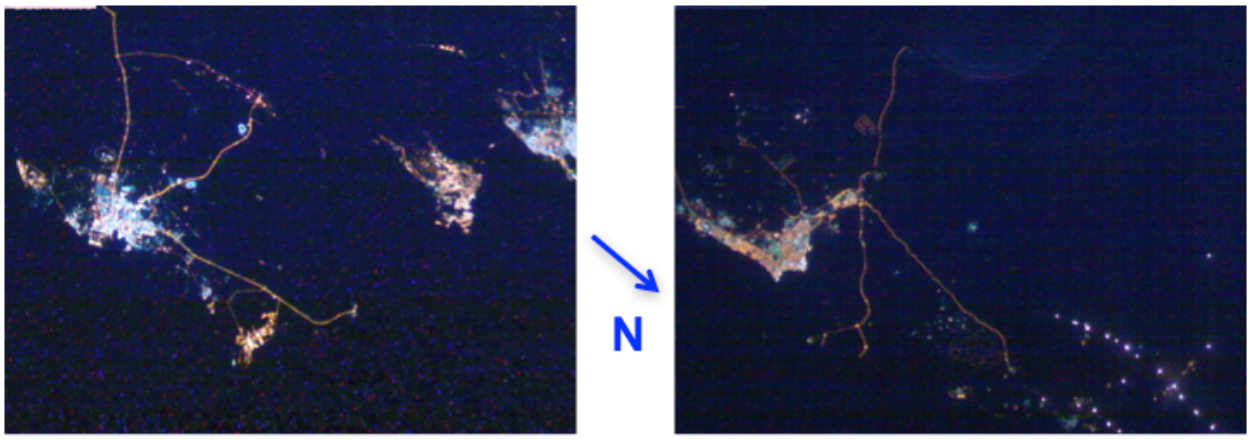

A **B**

Figure 4. Two frames from the 11 May 2015 Persian Gulf AC-5 Experiment. A. 23:28:46UT Qatar, Bahrain and the Coast of Saudi Arabia. B. 23:30:11 UT Kuwait City/Iraqi Border Gas Flares. Lunar Data Were: 25.2° Altitude, 115° Azimuth, 44% illuminated (20.6°, 114°, 44% for Kuwait City

2.5 Observations of Other Cities with AeroCube-5

We tasked the AC-5 NFOV camera to look at a number of other highly developed urban areas outside of the interesting and often cloud-free Persian Gulf region. Some examples are shown in Figures 5 and 6. Figure 5 shows imagery of Beijing and Tianjin in China and Osaka in Japan taken on the nights of 29 April and 2 May 2015. In Fig. 5A, the Beijing area of the image shows evidence of fuzziness from thin clouds, but no obvious cloud structure from scattered moonlight. Beijing International Airport stands out, as do the major transportation corridors on the way to Tianjin and the port area at the coast. There is some streaking of light features as well, suggesting the pointing maneuver did not work as well for this image sequence. Figure 5 B shows a cloudy moonlit scene of the Osaka Bay region. The city lights here also have a "fuzzy" appearance, but cloud structures from the light scattered from the full Moon are clearly visible. The sweep of the Bay is evident from the distribution of lights on the shoreline. Major features of the transportation grid are evident, as is the Yodo River, and both international airports, notably Kansai International Airport built on a man-made island in the bay southwest of Osaka. Again, there is some streaking of the lights in this image, making it of lower quality than our AC-5 Persian Gulf data. These images are presented to show some of the diversity in our results. Cloud impacted images are inevitable, but with the sensitivity of the AC-4 and AC-5 cameras, are only plainly obvious when the moon is full.

Figure 6 shows two images of cities in the United States. The first, Fig. 6A, is a frame from a sequence of images taken of the Chicago area. Excellent visibility of the lights of Chicago, major transportation corridors and outlying communities is evident, especially the I-90 linking Rockford, IL to the northwest. Major features include the Lake Michigan boundary on the North side of the image. No obvious lunar illumination scattered from the dark agricultural and forested areas in the region is observed, and no clouds are observed. The second image in Fig. 6B is a frame from a sequences of images along the East Coast of the United States. Philadelphia and the New York City area are notable with the connecting I-95 corridor linking them. The bright lights of Manhattan are evident, framed by the Hudson River and East River, with the dark area of Central Park also noticeable. No lunar illumination is observed.

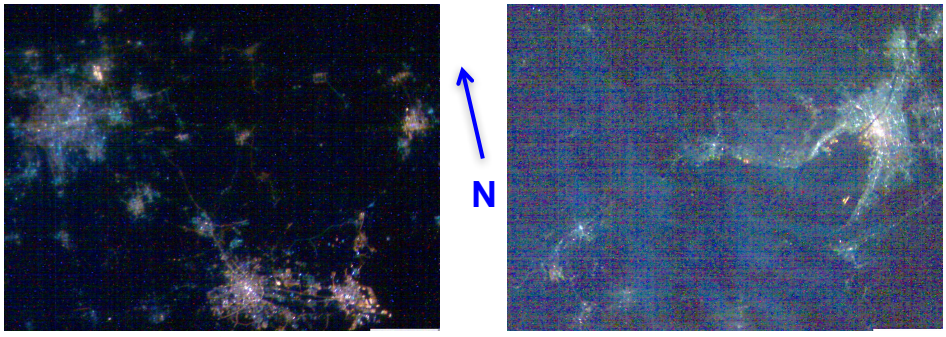

A **B**

Figure 5. AC-5 City Imagery. A. 29 April 2015 Beijing and Tianjin 16:07:46 UT. B. 02 May 2015 Osaka 15:55:16 UT. Lunar data were: A. 32.8° Altitude, 241°Azimuth, 82% illuminated, and B. 37.3° Altitude, 220.1° Azimuth, 98% illuminated

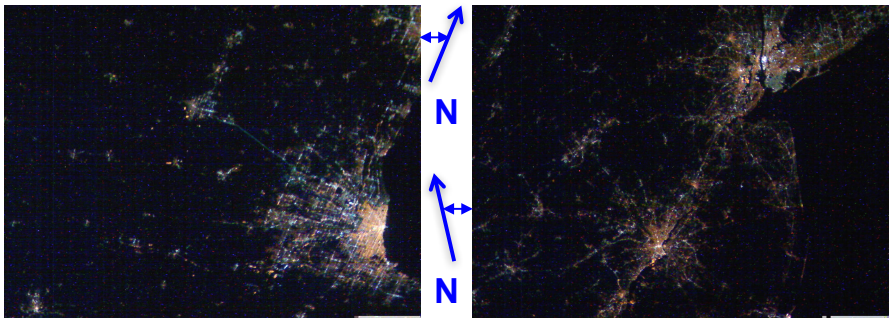

A **B**

Figure 6. AC-5 City Imagery. A. 1 May 2015 Chicago 05:43:12 UT. B. 31 October 2015 Philadelphia and New York City 04:49:01 UT. Lunar data were: A. 37.0° Altitude, 218°Azimuth, 92% Illuminated, and B. 41.4° Altitude, 103° Azimuth, 82% Illuminated.

2.6 Comparisons of Imagery Obtained with the AeroCube Camera to ISS Photography

Based on ground sample distance alone, the higher resolution observations possible with the NFOV camera on AC-5 approach, but do not meet, the 50-100 m resolution requirement identified in the Nightsat mission concept work.[10] This is the resolution at which nightlights images begin to resolve structure on the scale of individual city blocks (~100 m). The NFOV camera is able to detect light gaps on the order of 200 m in moderately illuminated urban regions. More precise characterization of the point-spread function of the NFOV camera is needed to better quantify performance. Designing an optimal future sensor will require balancing sensitivity, resolution, geographical coverage, multi-spectral capability if desired, and accommodating the sensor within an affordable spacecraft. We have shown that accurately pointed 1U and 1.5U spacecraft with tiny cameras built from commercially available parts can approach the capabilities needed for monitoring of city-sized areas.

We undertook qualitative comparison of our AeroCube camera data to NASA/ESA ISS photography. We were impressed by the quality of the best ISS nighttime photography, especially the recent work with the ESA Nightpod motion compensation system when combined with high-end NIKON cameras and large fast lenses.[11-13] We were able to document the AeroCube Camera's ability to detect new urban developments via nighttime lights at the multi-block neighborhood, or large facility level, when compared to older Nightpod-stabilized ISS photography that resolves down to 50 meters or better. Some examples of this work, including the changes detected between ISS images, taken in 2012, 2013, and AeroCube images, taken in 2015, will be presented in the briefing chart submission to the conference workshop. Figure 7 shows image chip comparisons between one of the highest quality ISS images we've examined and one of our best AC-5 NFOV camera images. The ISS camera in this example was a Nikon D3S equipped with an *f*/2.8 180 mm lens.[12]

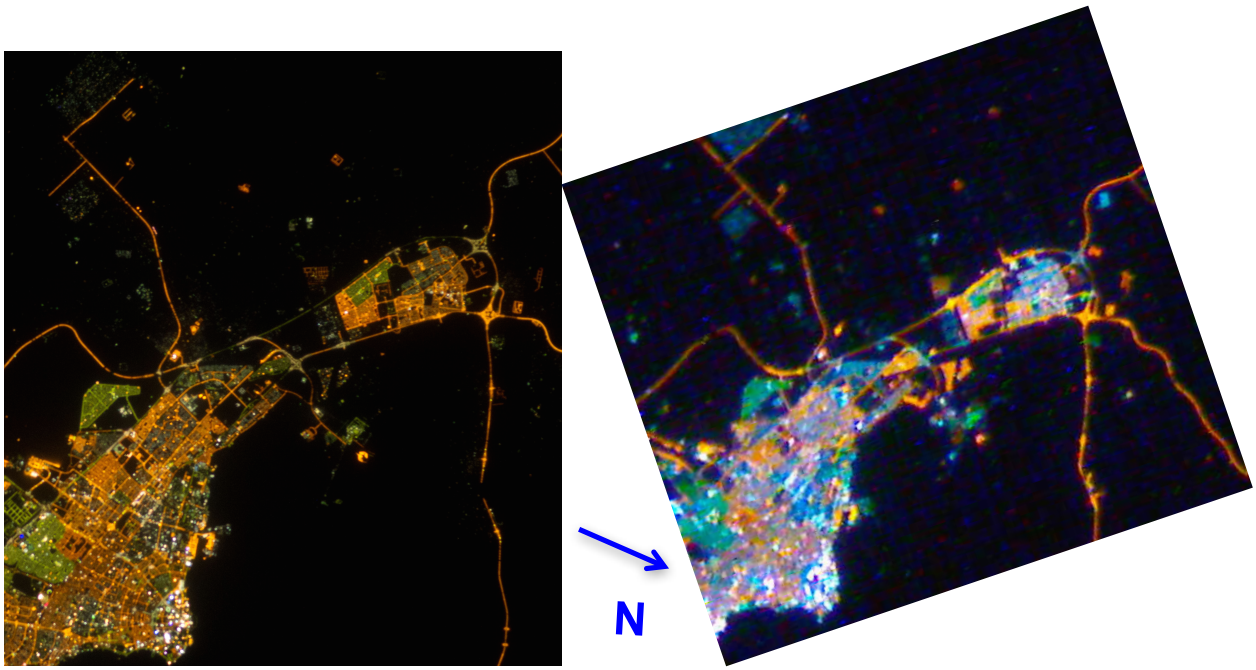

A **B**

Figure 7. Comparison of ISS and AeroCube Photography. A. ISS Image 12 February 2013 at 21:51:44 UT. B. AC-5 NFOV Image 28 June, 2015 22:27:04 UT. Image width is ~45 km. Lunar data were: A. Moonset 16:55 UT, and B. 12.0° Altitude, 243° Azimuth, 89% Illuminated

3.0 Future Efforts

The work in this paper was done with cameras on experimental AeroCube satellites that were devoted to improving the CubeSat bus in all its aspects: power, communications, pointing, and related topics. Care was put into the design of the cameras, but their main goals were as daytime pointing verification tools to test the attitude control system, as well as first steps towards future star tracking cameras. CubeSats have been constructed and will soon be launched which will have more capable cameras on board. These include two

OCSD/AC-7 CubeSats and the ISARA CubeSat which hosts the CUMULOS payload (OCSD is the NASA Optical Communications and Sensor Demonstration, also referred to as AeroCube-7, ISARA is the JPL Integrated Solar Array and Reflectarray Antenna, a 3U CubeSat which hosts the CUbesat MULtispectral Observation System, an Aerospace Corporation sensor). All of these will deploy from the Falcon-9 v1.1 rocket scheduled to launch Formosat-5. The launch is currently scheduled for October 2016 and will host a number of other CubeSat payloads.

The Optical Communications and Sensor Demonstration (OCSD, also known as AeroCube-7) satellites have several cameras on-board including one with an *f*/1.9 35mm lens and a 3856 x 2764 pixel RGB Bayer pattern CMOS array. Some key camera parameters are documented in Table 2. This program was reported on in more detail at the 2015 SmallSat conference.[14] The ISARA spacecraft hosts an auxiliary sensor, the CubeSat Multispectral Observation System, or CUMULOS. This payload consists of three cameras: a visible 0.4-0.9 µm monochromatic CMOS camera, a 0.9-1.7 µm SWIR InGaAs Camera, and a 7.5-13.5 µm LWIR microbolometer camera, all of which fit into less than 1.5U of a 3U CubeSat. The CUMULOS sensor can be thought of as a tiny weather satellite aimed at some of the nighttime missions associated with VIIRS (nighttime lights and hotspots). It will fly a microbolometer as a cloud detector and surface temperature sensor. These cameras went through pre-flight ground calibration at flight temperatures, and in-flight calibration tests are part of the project goals. This sensor will be more fully described at the AIAA/USU Calibration Conference in August, 2016.

Table 2 summarizes some relevant camera parameters for these upcoming payloads. The AC-7 camera will give a higher resolution capability, at the cost of some area source sensitivity. The OCSD spacecraft tests a laser communications payload that increases downlink capability, hopefully allowing for more experiments. The CUMULOS VIS and SWIR cameras will enhance our sensitivity by approximately 1 and 2 orders of magnitude relative to the AeroCube cameras we used in this work and will provide near simultaneous multispectral data. It is our intention to extend our nighttime lights research with joint observations from these systems that will complement each other and help us extend the work summarized in this paper using higher resolution cameras, more sensitive, calibrated cameras, and nearly simultaneous data in multiple spectral bands. Results will be used to aid in the design of a future optimal NightCube mission.

Table 2. Camera Parameters for Related Soon-To-Be-Launched Aerospace Payloads

Satellite Camera	Lens *f*#	Lens Focal Length (mm)	Pixel Pitch (µm)	Nominal Altitude (km)	GSD (m)
AC-7 (high res)	1.9	34.9	1.67	600	28.7
CUMULOS VIS	1.4	17.6	5.20	600	177
CUMULOS SWIR	1.4	25.0	25	600	600
CUMULOS LWIR	1.1	25.0	17	600	408

Acknowledgements

This research was funded by The Aerospace Corporation's Internal Research and Development program. The authors also wish to acknowledge the U.S. Air Force Space and Missile Systems Center Advanced Development Directorate (SMC/AD), and the Multi-Program Acquisition Capability Enhancement Program (MPACE), for their support of AeroCube-4 and the CUMULOS payload.

References

1. Elvidge, C. D., Ziskin, D., Baugh, K. E., Tuttle, B. T., Ghosh, T., Pack, D. W., Erwin, E. H., Zhizhin, M., "A Fifteen Year Record of Global Natural Gas Flaring Derived from Satellite Data", Energies, vol. 2, no. 3, 2009.
2. Elvidge, C.D, Zhizhin, M., Baugh, K., Hsu, F.-C., Ghosh, T., "Methods for Global Survey of Natural Gas Flaring from Visible Infrared Imaging Radiometer Suite Data", Energies, vol. 9, January 2016.
3. Miller, S.D, Mill, S.P., Elvidge, C.D., Lindsey, D. T., Lee, T.F., Hawkins, J.D., "Suomi Satellite Brings to Light a Unique Frontier of Nighttime Environmental Sensing Capabilities", Proceedings of the National Academy of Sciences, vol. 109, no. 39, September, 2012.
4. Miller, S.D., Straka III, W., Mills, S., Elvidge, C., Lee, T., Solbrig, J., Walther, A., Heidinger, A., Weiss, S., "Illuminating the Capabilities of the Suomi National Polar-Orbiting Partnership (NPP) Visible Infrared Imaging Radiometer Suite (VIIRS) Day/Night Band", Remote Sensing, vol. 5, 2013.
5. Elvidge, C.D.; Hsu, F.-C.; Baugh, K.; Ghosh, T., "Why VIIRS data are superior to DMSP for mapping nighttime lights", Proceedings of the Asia-Pacific Advanced Network v. 35, 2013.

6. Elvidge, C.D.; Hsu, F.-C.; Baugh, K.; Ghosh, T., "National Trends in Satellite Observed Lighting: 1992–2012", In Global Urban Monitoring and Assessment through Earth Observation; Weng, Q., Ed.; CRC Press: Boca Raton, FL, USA, pp. 97–120, 2014.
7. Gangestad, J.W., Rowen, D.W. and Hardy, B.S., "Forest Fires, Sunglint, and a Solar Eclipse: Responsive Remote Sensing with AeroCube-4", Geoscience and Remote Sensing Symposium (IGARSS), IEEE, Quebec City, Canada, July 2014.
8. Gangestad, J.W., Rowen, D.W. and Hardy, B.S., "Along for the Ride: Experience with Flexible Mission Design for CubeSats", Proceedings of the AIAA/AAS Astrodynamics Specialist Conference, SPACE Conferences and Exposition, San Diego, CA, August, 2014.
9. Gangestad, J.W., Rowen, D.W., Hardy, B.S. and Hinkley, D.A., "Flying in a Cloud of CubeSats: Lessons Learned from AeroCube-4, -5 and -6", Proceedings of the 65 International Astronautical Congress, Toronto, Canada, September, 2014.
10. Elvidge, C.D, Cinzano, P., Pettit, D.R., Arvesen, J., Sutton, P., Small, C., Nemani, R., Longcore, T., Rich, C., Safran, J., Weeks, J, Ebener, S. "The Nightsat Mission Concept", International Journal of Remote Sensing, vol. 28, No. 12, May 2007.
11. Kyba, C.C.M., Garz, S. Kuechly, H., De Miguel, S.A., Zamorano, J., Fischer, J., Hölker, F., "High-Resolution Imagery of Earth at Night: New Sources, Opportunities and Challenges", Remote Sensing, vol. 7, January 2015
12. All photographs taken from the International Space Station and their meta data are available at "The Gateway to Astronaut Photography of Earth", which is run by NASA: http://eol.jsc.nasa.gov.
13. De Miguel, S.A.; Castaño, J.G.; Zamorano, J.; Kyba, C.C.M.; Pascual, S.; Ángeles, M.; Cayuela, L.; Martin Martinez, G.; Caltner, P., "Atlas of astronaut photos of Earth at night" Astronomy and Geophysics, vol. 55, no. 4 August 2014. This helpful Atlas to nighttime ISS photography is described by Kyba et. al. in reference 11 and online at: http://www.citiesatnight.org, and http://www.nightcitiesiss.org/
14. Janson, S.W., Welle, R., Rose, T., Rowen, D., Hinkley, D., Hardy, B. La Lumondiere, S., Maul, G., Werner, N. "The NASA Optical Communication and Sensors Demonstration Program: Preflight Update", Proceedings of the 29th Annual AIAA/USU Conference on Small Satellites, Logan, Utah, USA, August, 2015.